atmosphere

MDPI

*Article*

# Spatio-Temporal Variability of Hydroclimatology in the Upper Cauca River Basin in Southwestern Colombia: Pre- and Post-Salvajina Dam Perspective

**Wilmar L. Cerón [1], Mary T. Kayano [2,*], Camilo Ocampo-Marulanda [3,4], Teresita Canchala [4], Irma Ayes Rivera [5], Alvaro Avila-Diaz [6,7], Rita V. Andreoli [8,9] and Itamara Parente de Souza [9]**

1 Department of Geography, Faculty of Humanities, Universidad del Valle, Calle 13 # 100-00, P.O. Box 25360, Cali 25360, Colombia; wilmar.ceron@correounivalle.edu.co
2 Coordenação Geral de Ciências da Terra, Instituto Nacional de Pesquisas Espaciais, Avenida dos Astronautas, 1758, São José dos Campos 12227-010, Brazil
3 Faculty of Natural Sciences and Engineering, Fundación Universitaria de San Gil, Unisangil, Yopal 850001, Colombia; camilo.ocampo@correounivalle.edu.co
4 Water Resources Engineering and Soil (IREHISA) Research Group, School of Natural Resources and Environmental Engineering, Universidad del Valle, Cali 25360, Colombia; teresita.canchala@correounivalle.edu.co
5 Independent Researcher, Tegucigalpa-61, Tegucigalpa 11101, Honduras; ayesrivera@hotmail.com
6 Facultad de Ingeniería, Universidad de Ciencias Aplicadas y Ambientales—UDCA, Bogotá 111166, Colombia; alavila@udca.edu.co
7 Natural Resources Institute, Universidade Federal de Itajubá, Itajubá 37500-903, Brazil
8 Escola Superior de Tecnologia, Universidade do Estado do Amazonas, Av. Darcy Vargas, 1200, Parque 10 de Novembro, Manaus 69065-020, Brazil; rasouza@uea.edu.br
9 Programa de Pós-Gradução em Clima e Ambiente, Instituto Nacional de Pesquisa da Amazônia, Manaus 69065-020, Brazil; ips.mcl16@uea.edu.br
* Correspondence: mary.kayano@inpe.br; Tel.: +55-12-3208-6658

**Abstract:** The Cauca River rises in the Colombian Andes and is the main tributary of the Magdalena River, which drains to the Caribbean Sea. The La Balsa station monitors the Upper Cauca basin and is located just downstream of La Salvajina hydroelectric facility. At this station, the discharge time series for November–January during 1950–2019 shows a statistically significant downward break, and change of distribution after 1986 has been documented after La Salvajina started operation. We assessed the spatio-temporal variability of hydroclimatology in the upper Cauca River basin during the pre- and post-Salvajina dam periods to better understand this break. Post-Salvajina, low (high) discharge events are linked to negative (positive) precipitation and soil moisture anomalies that are greater in magnitude and extension than those recorded in the pre-Salvajina period in response to the more intense El Niño events (more intense and frequent central La Niña events) after 1986. Therefore, it is necessary to consider possible future rainfall scenarios and non-infrastructure measures (i.e., reforestation, territorial planning, integrated watershed management, etc.) to mitigate floods and droughts impacts. The contribution of this study is to provide evidence for the need for foresight in the design of any structural or non-structural flood measures.

**Keywords:** Cauca river basin; La Salvajina; climate variability; water discharge



**Citation:** Cerón, W.L.; Kayano, M.T.; Ocampo-Marulanda, C.; Canchala, T.; Rivera, I.A.; Avila-Diaz, A.; Andreoli, R.V.; de Souza, I.P. Spatio-Temporal Variability of Hydroclimatology in the Upper Cauca River Basin in Southwestern Colombia: Pre- and Post-Salvajina Dam Perspective. *Atmosphere* **2021**, *12*, 1527. https://doi.org/10.3390/atmos12111527

Academic Editor: Indrani Roy

Received: 20 October 2021
Accepted: 16 November 2021
Published: 19 November 2021



## 1. Introduction

In northwestern South America, the Cauca River Basin (CRB) is the second most important surface water source in Colombia, crossing the western part of the country, which has a high water demand for the domestic, agricultural, and industrial supply [1]. Notably, the upper CRB is geo-strategically of special importance, given that it includes most of the productive chains prioritized for Colombia ranging from small farms to extensive industries, including the sugar industry, coffee crops, power generation, mineral extraction,

and agriculture [2–4]. Furthermore, this region presents a complex ocean-land-atmosphere dynamic modulated by several factors which, acting with local processes, are determinant to the hydro-climatological variability in the CRB [5]. Among these factors, the meridional migration of the Intertropical Convergence Zones (ITCZ) of the Atlantic and Pacific Oceans, the moisture transport from the Amazon basin, the trade winds and the topography characterized mainly by the inter-Andean valley shaped by the Cauca River between the western and central Colombian mountain ranges stand out [5–10].

The CRB is influenced by oceanic-atmospheric phenomena of complex understanding, such as the El Niño Southern Oscillation (ENSO). This causes a high frequency of occurrence of extreme events associated with hydrological hazards (e.g., floods, droughts) [4,11,12]. Several studies show specific evidence of the ENSO influence on the north of South America [13–22], where the CRB is located, with a decrease in precipitation during the warm ENSO (El Niño) phase and an increase during the cold ENSO (La Niña) phase. Furthermore several hydro-climatological studies carried out in the CRB have registered floods [23,24] and droughts [3,12,25], in addition to the historical records of hydrometeorological disasters in the region [4,26]. Even though these hydroclimatic events are part of the natural variability, they can endanger the economic and social development of the region [2–4,12,27]. The consequences of these threats range from flooding over vast territories dedicated to agriculture and livestock, urban and rural areas, with the partial or total destruction of existing infrastructure [15,16,27], to droughts with devastating effects on agriculture and livestock, ecological and urban/rural systems, energy deficits, among others [2,3,12,13,28,29].

In this sense, several structural measures have been implemented in the upper CRB since the 1950s to manage extreme events. These included the RUT Irrigation District (RUT for its acronym in Spanish, also refers to the Roldanillo, La Unión, and Toro municipalities), the Aguablanca project, and the "Cauca River Regulation project" [27]. This last project included the construction of the Salvajina Dam (hydropower plant) approved by the Corporación Autónoma Regional del Valle del Cauca (CVC) in 1978, which became operational in September 1985. The dam was constructed to control flooding in the valley's flat zone, alleviate the contamination of the river during low water levels through the dilution of sediments, and produce 187.5 GWh [30] integrated into the Interconnected Energy System [31]. According to the inventory of flood disasters in Cali, the Salvajina brought positive impacts to mitigate the effects of flooding of the CRB, showing a reduction in the frequency and magnitude of these catastrophic events after 1985 [32].

Nevertheless, some studies point out that, despite these efforts, the management of floods in the Upper CRB is still not adequate and, therefore, their effects are very hazardous [4,26,27]. Enciso et al. [4] identified large floods between 1988 and 2011, indicating that Salvajina Dam has decreased its ability to regulate floods in the upper CRB. Furthermore, the impact of flooding has been aggravated due to the gradual desiccation of the wetlands along the basin, which act as natural buffers for floods. According to Perafán-Cabrera [33] and Ocampo-Marulanda et al. [26], in Colombia 24.2% of wetland areas present severe damage, and 87.7% of the wetland area in the Valle del Cauca state (upper CRB) has disappeared due to the desiccation process. Moreover, the imminent increase trends in deforestation in Colombia Andes cause disturbances in hydrological regimes, intensifying the impact and magnitude of the hydrological hazards [23,34,35]. Solely between 2005–2010, Restrepo et al. [36] described a forest loss of 100,000 ha year$^{-1}$ in the CRB, the highest deforestation rate compared to the other tributaries of the Magdalena River.

The natural climate variability and the expected changes in ENSO feature in the last few decades, due possibly to global warming [37–39], and linked to the decadal changes in the climate throughout the Pacific basin [40–42] could reduce the capability of flood-control infrastructures and increase of the negative effect of floods and drought. Indeed, the ENSO anomalies might be responsible for up to 65% of the interannual streamflow variability in the CRB [30,43]. For instance, between 2010 and 2011, two catastrophic events in the Colombian Andes happened with 440 km$^2$ and 393 km$^2$ flooded areas. These events

occurred during La Niña 2010–2011. The damage caused in this period amounts to 0.12% of Colombia's Gross Domestic Product [18,44]. According to the Government of Colombia's National Administrative Department of Statistics (DANE; https://www.dane.gov.co/ (accessed on 17 May 2021) more than 230,225 people were affected by this event. These results are consistent with those presented by Poveda et al. [45] and Sedano-Cruz [46], who identified and demonstrated the strong influence of ENSO on hydrology, especially on the flows of flooding in Colombia. Recently, Avila et al. [23] identified positive trends during December–February in extreme precipitation indices in the CRB from 1970 to 2013, especially in the central region (3°–4° N).

Moreover, during the 2015–2016 El Niño event [47,48], 40% of rainfall deficits occurred in the Colombian Andean region, recording historical maximum temperatures, droughts, forest cover fires, as well as a decrease in flows to historically low levels for the main rivers of the Andean region (including the upper CRB, see Figure 1a); besides direct effects on productive sectors, such as livestock production, which saw a decrease in milk and meat production, during the May 2015–January 2016 period partial losses in the livestock sector amounted to $632 billion, and more than 1 million hectares of crops were affected [49].

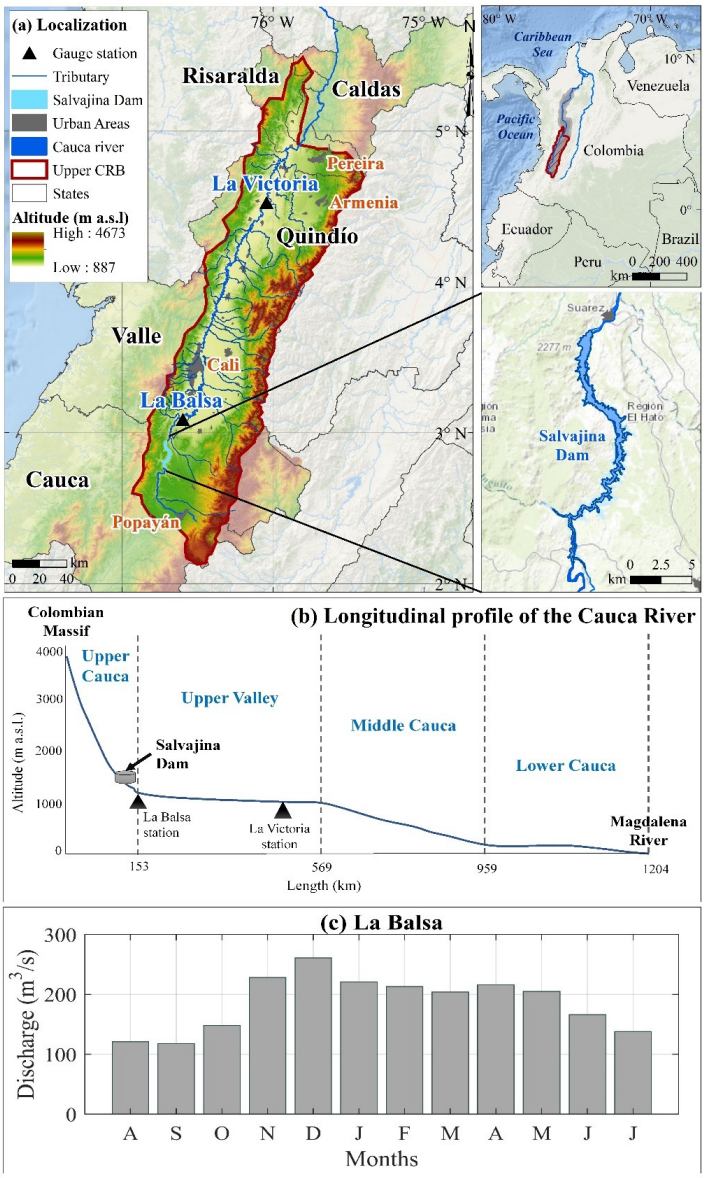


**Figure 1.** (**a**) Upper Cauca River Basin localization and study stations, (**b**) longitudinal profile of the Cauca River, and (**c**) annual discharge cycle at La Balsa station from 1949–2019.

Given the CRB's importance for Colombian socio-economic development and with the intention of improving risk management, this study aims to assess the spatio-temporal variability of hydroclimatology in the Upper CRB in Southwestern Colombia during pre and post-Salvajina Dam. On a monthly scale, we identify the years with intense discharge in the Upper CRB and examine the related anomalous oceanic and atmospheric patterns and their impacts on precipitation and soil moisture, focusing mainly on the November–January (NDJ) peak discharge during the last six decades (1949–2019). The study area and its principal socio-economical features are described in Section 2, and the observed climate data, statistical methods, and experimental design are described in Section 3. The variations in historical discharge and the influence of the climate variables pre- and-post-Salvajina are evaluated in Section 4. Concluding remarks comprise Section 5.

## 2. Study Area

The Cauca River rises in the paramo of the Colombian Massif, flowing in a south-north direction between the Western Cordillera and the Central Cordillera of the Andes mountain, ranges for approximately 1183 km until its confluence with the Magdalena River (Figure 1a), covering an area of 66,751 $km^2$ with an annual water discharge of 76 $km^3$ per year [36]. It is fed by the tributary rivers that originate in the Central and Western Cordillera of the Andes. Four zones are identified through the river course: Upper Cauca, Upper Cauca Valley, Middle Cauca, and Lower Cauca (Figure 1b) [50].

In the upper CRB (Upper Cauca and Upper Cauca Valley), approximately 7 million Colombians live, which corresponds to 15% of the national population [51]. Its agricultural vocation characterizes the area with sugarcane crops to the south in the plain of the Cauca River valley and coffee crops to the north in the mountainous area [52]. The Upper Cauca River has a mean annual discharge of 188 $m^3/s$ at La Balsa and 381 $m^3/s$ at La Victoria gauge stations (Figure 1a). There is a 102% increase in discharge between the two stations due to the 27 rivers that flow into the Cauca River along this section. On the other hand, the afferent area of the Cauca River at La Balsa is 4396 $km^{2,}$ and La Victoria is 18,244 $km^2$, which is consistent with the difference in discharge. The study area represents 569 km of the Cauca River's course (about 48%) from its headwaters to the Victoria gauge station, representing 68% (18244 $km^2$) of all the CRB. The Upper Cauca River extends from its source to the La Balsa station (Figure 1b) with a 19.60 m per kilometer slope. This reduces to 0.24 m per kilometer at the piedmont of the Upper Cauca Valley. The longitudinal profile and altitudes can be observed in Figure 1b.

In the Upper Cauca, the Salvajina Dam has been in operation since 1985 with a capacity of 866 $hm^3$ (see location in Figure 1a,b). This dam was conceived with the primary objective of regulating the CRB and downstream flood control [4]; additionally, the dam fulfills other functions such as power generation and water quality improvement of the river. The dam was one of the elements that transformed the Cauca riverbed in the Upper Cauca Valley; other infrastructure works included dikes, interceptor canals, pumping stations, and drainage canals [26].

According to Puertas et al. [52] and Cerón et al. [53], the region has a mean annual rainfall of 1597 mm (±224 mm) and a mean air temperature of 21.3 °C (±0.5 °C). Thus, rainfall and temperature present an inverse behavior with a bimodal intra-annual variability with two rainy periods in the March–April–May (MAM) and September–October–November (SON) quarters, as well as two less rainy periods during the December–January–February (DJF) and June–July–August (JJA) quarters. This bimodal rainfall pattern is attributed to the influence of the trade winds and the ITCZ migration through the study area in a south–north direction during the first half of the year and subsequently in a north–south direction during the second half [28,53,54].

## 3. Materials and Methods

### *3.1. Hydrological Data*

Monthly water discharge (Q) at La Balsa from 1949 to 2019 was used. This information is provided by the CVC and is available online at: http://ecopedia.cvc.gov.co/modulo-consulta (accessed on 15 May 2021). The monthly data were consistent and showed less than 10% missing values for the time span. The hydrological year from August to December ($year_{t-1}$) to July to September ($year_{t0}$) was used for the analysis. Afterward, the interannual time series was generated for the peak discharge at La Balsa station, corresponding to the quarter from November to January (NDJ). Large floods were recorded between November and January in this basin, 10 of 15 events with peak water discharges between 800 and 1060 $m^3/s$ at La Balsa station (1950–2011) [55]. Thus, the discharge series were analyzed considering the peak discharge in NDJ.

### *3.2. Atmospheric and Oceanic Information*

For this study, we used sea surface temperature (SST), sea level pressure (SLP), zonal (u) and meridional (v) winds at 925 hPa, precipitation (PRP), and surface soil moisture volume (SMV) during the period 1950–2019, derived from the ERA5 reanalysis [56]. SST data were obtained in the region between 40° N–40° S, 120° E, and Greenwich, SLP and u and v winds at 925 hPa between 40° N–10° S and 120° W–10° W, precipitation and SMV in the domain within 20° N, 10° S, 60° W, and 90° W. ERA5 is the fifth ECMWF reanalysis generation that incorporates a detailed record of global atmospheric, oceanic, and land surface phenomena since 1950 and replaces the ERA-Interim reanalysis [57]. Its hourly output, the high horizontal resolution of 31 km, and 137 pressure levels (land surface down to 0.01 hPa) provide significantly finer details of oceanic and atmospheric phenomena relative to previous global reanalyses [56,57].

ERA5 integrates model data with observations across the globe into a coherent, global dataset using so-called data assimilation to produce a best new estimate of the state of the atmosphere, called an analysis, resulting in an updated and improved forecast. The ERA5 is updated daily with a latency of 5 days. The data have been regrouped into a regular latitude-longitude grid of 0.25° and are available for monthly averaged data on pressure and individual levels https://cds.climate.copernicus.eu/cdsapp#!/search?type=dataset (accessed on 17 May 2021). This reanalysis has been used in recent studies of extreme event trends associated with climate variability and climate change [58–60], surface wind speed, and variability in the South American region [61,62], and land-atmosphere interactions [63].

Furthermore, we used precipitation data derived from the Global Precipitation Climatology Center (GPCC) Full Data Monthly Product Version 2020 [64,65] to examine consistency with ERA5. GPCC is a gauge-based gridded monthly precipitation dataset for the global land surface; it is available in 2.5°, 1°, and 0.5° spatial resolutions. For this study, we used the horizontal resolution of 1°, and the 1950–2019 period was selected for all variables. Data are collected by the World Meteorology Organization (WMO) from each country to GPCC or are calculated from the monthly time series available from the GPCC database; for more information about the database, please refer to the following web page https://opendata.dwd.de/climate_environment/GPCC/full_data_monthly_v2020/10/ (accessed on 1 June 2021).

Moreover, we calculated the monthly precipitation index for the upper CRB, corresponding to the average of the ERA5 pixels within the region upstream of the La Balsa station (Figure 1a), used to analyze consistency and relationships with the discharge.

### *3.3. Discharge Variability Pre- and Post-Breaking Point*

Our hypothesis is that, besides the effect of dam to control flows in the upper CRB, climatic variability played a crucial role in the discharge modulation after the beginning of the Salvajina's operation (1985). Therefore, discharge times-series generated at the quarterly time step were finally evaluated to seek breaks and temporal trends for the 1950–2019 period. For this, we applied the following statistical tests: (1) the non-parametric Pettitt

test to seek breaks along with the time series [66], estimating the *p*-values using Monte Carlo resampling; in these tests, the null hypothesis (H0) that no rupture exists in the time series is tested against the alternative hypothesis (H1), with changes in the mean; if a break is obtained, the following tests are performed; (2) the Mann-Whitney test [67] to investigate changes in the distribution; and (3) the statistical non-parametric Mann-Kendall test to evaluate temporal trends over the time series [68,69]. The time series linear trend was calculated using Sen's slope (β) estimator [70–72]. Outcomes with 95% confidence intervals are shown in the results section. The Mann-Kendall and Sen's slope tests are non-parametric methods applied to detect trends and magnitudes of deviations in time series data [23,58,73,74]. Additional details on the equations and procedures adopted in these methods can be found in the studies by [75,76]. All statistical tests were performed with MATLAB R2021b. The subroutines used in this work include: for Pettitt test [77], for Mann-Kendall test [78], for Theil–Sen estimator [79], and for Mann-Whitney test [80].

Once a breakpoint was detected, the discharge series percentiles during NDJ were used to classify the high and low flow events at La Balsa, separating them for the periods before and after the breakpoint. Thus, high events are above the 75th percentile and low events below the 25th percentile for each period. Furthermore, we used the Oceanic Niño Index (ONI) to examine the relationships between La Niña and El Niño events with high or low flow events, pre- and post-breaking point. The ONI is available at https://origin.cpc.ncep.noaa.gov/products/analysis_monitoring/ensostuff/ONI_v5.php (accessed on 27 October 2021).

Furthermore, we used composite analysis to establish the oceanic and atmospheric patterns associated with positive and negative pre- and post-breakpoints events. This method has been used extensively in recent decades to identify conditions observed during specific climate states and provides valuable information on the physical mechanisms involved [11,22,23,81]. For the years before and after the breakpoint, composites were calculated separately for standardized anomalies of SST, SLP, PRP (including GPCC and ERA5), SMV, and 925 hPa winds. Composite analysis is a commonly used tool for identifying the mean patterns and variations related to a particular phenomenon [58,82–84]. This technique consists in calculating the arithmetic mean of the anomalies corresponding to the selected events following the selection criteria described above [82]. The equation of the composites is expressed by Equation (1)

$$\psi_c(i,j) = \frac{1}{N}\sum_{n=1}^{N}\psi_{CE}(i,j,n) \quad (1)$$

where $\psi_C$ represents the mean of all composite fields, $\psi_{CE}$ represents a composite field, with $i$, $j$ representing the grid points, of the n-th events $n$ and $N$ the number of events [85].

Statistical significance of the composites was evaluated using Student's $t$-test for significance of the means [85,86]. We considered the degrees of freedom as the number of events in each period, and the significance was evaluated by applying a 95% confidence level. The Student's $t$-test is given by Equation (2)

$$T = \frac{\overline{X} - \mu_0}{\frac{\sigma}{\sqrt{n}}} \quad (2)$$

in which $\overline{X}$ is the mean, $\mu_0$ is the population mean under null hypothesis, $\sigma$ is standard deviation, and $n$ is the size of the series [85].

Before any calculations, the linear trend was removed from the time series, using the least-squares method, resulting in the monthly standardized anomalies being converted to the de-trended anomalies. Thus, the trends, monthly means, and standard deviations correspond to these operations' 1950–2019 base period.

## 4. Results and Discussion

### *4.1. Discharge Variability*

The discharge time series for NDJ over the 1950–2019 period depicted in Figure 2 was tested with the Pettitt test, showing a statistically significant breakdown in 1986, a year after the Salvajina Dam was put into operation, such that the NDJ mean discharge before this breakdown of 281 $m^3/s$ contrasts with a mean discharge of 209 $m^3/s$ after the breakdown (Figure 2). This seasonal discharge variation during NDJ at La Balsa station indicates less pronounced maximum flow peaks and lower minimum flow peaks post-Salvajina in 1986 (Figure 2) and is depicted by the Mann-Whitney test with a change in the interannual NDJ distribution ($p < 0.001$). On the other hand, from this breakpoint, we performed the Mann-Kendall test and the magnitude calculation from Sen's slope estimator for both periods separately, finding non-significant results (Figure 3).

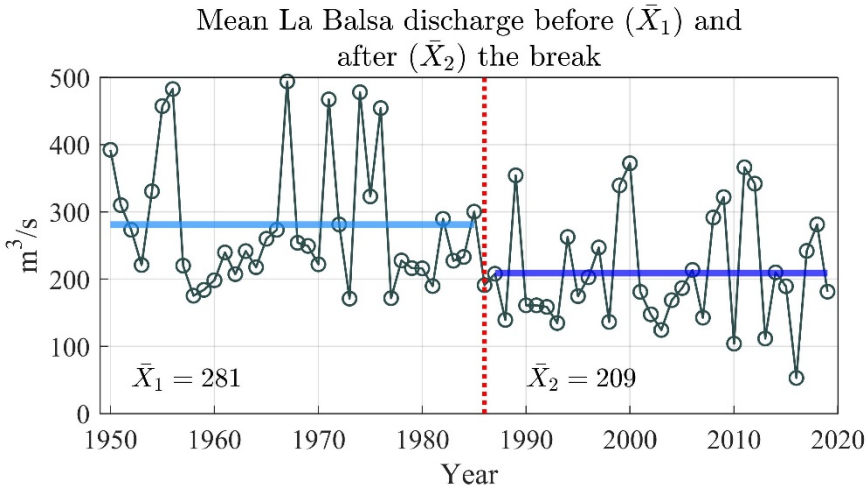


**Figure 2.** Mean La Balsa discharge time series from November to January (NDJ) during the 1950–2019 period (solid line). According to the Pettit test, the vertical red dashed line indicates the break year (1986), significant at the 0.05 significance level. The two horizontal lines represent the mean discharge value before ($\overline{X}_1$) and after ($\overline{X}_2$) the break.

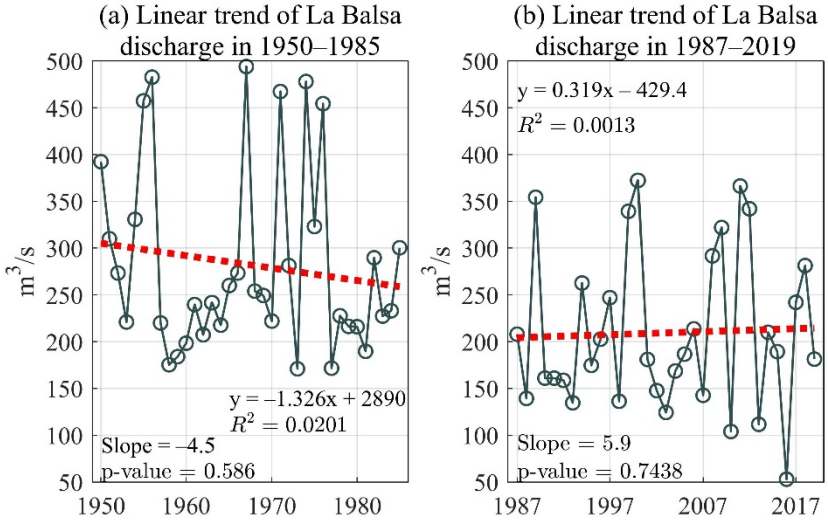


**Figure 3.** (**a**) Linear trend of La Balsa discharge during 1950–1985 period, and (**b**) during 1987–2019 period from November to January (NDJ). The red dotted line represents the linear trend of the discharge time series for each period.

These results agree with Enciso et al. [4], who found five historical flows in the upper CRB despite the implementation of La Salvajina, which resulted in floods in the second

half of the year for the 1988–2011 period, all associated with strong La Niña phenomena, which coincide with five of the maximum discharge events found after 1986 at La Balsa station (Table 1 and Figure 2). Thus, the strong influence of ENSO on the hydrology of the study area, especially on flood discharge in Colombia, is demonstrated.

**Table 1.** Intense flow events pre- and post-Salvajina Dam. LN is for La Niña events and EN for El Niño (ENSO) events. According to the ONI Index, available at https://origin.cpc.ncep.noaa.gov/products/analysis_monitoring/ensostuff/ONI_v5.php (accessed on 27 October 2021), W is for weak events, M for moderate, S for strong and vs. for very strong. N relates to neutral years.

| | High | Mean Discharge ($m^3/s$) | ENSO Type | Low | Mean Discharge ($m^3/s$) | ENSO Type |
|---|---|---|---|---|---|---|
| Pre-Dam Period | 1953–54 | 331 | W-EN | 1957–58 | 175 | S-EN |
| | 1954–55 | 457 | W-LN | 1958–59 | 184 | W-EN |
| | 1955–56 | 483 | M-LN | 1959–60 | 198 | N |
| | 1966–67 * | 494 | N | 1961–62 | 207 | N |
| | 1970–71 * | 467 | M-LN | 1972–73 | 171 | S-EN |
| | 1973–74 * | 478 | S-LN | 1976–77 | 172 | W-EN |
| | 1974–75 * | 323 | W-LN | 1979–80 | 216 | W-EN |
| | 1975–76 | 454 | S-LN | 1980–81 | 190 | N |
| Post-Dam Period | 1988–89 * | 354 | S-LN | 1987–88 | 139 | S-EN |
| | 1998–99 * | 339 | S-LN | 1992–93 | 135 | N |
| | 1999–00 | 372 | S-LN | 1997–98 | 136 | VS-EN |
| | 2007–08 | 292 | S-LN | 2002–03 | 124 | M-EN |
| | 2008–09 * | 322 | W-LN | 2006–07 | 143 | W-EN |
| | 2010–11 * | 366 | S-LN | 2009–10 | 104 | M-EN |
| | 2011–12 * | 342 | M-LN | 2012–13 | 112 | N |
| | 2017–18 | 281 | W-LN | 2015–16 | 53 | VS-EN |

* Historical events coinciding with the historical flooding events found by Enciso [4] and CVC [55].

Table 1 shows the years with intense high and low discharge events before and after the breaking point in 1986 (Figure 2). Pearson's coefficient showed a correlation of 0.70 between total rainfall and total discharge for the NDJ quarter. Hence, the mean annual rainfall and discharge cycles during high and low discharge events pre- and post-breaking point were analyzed compared to annual cycles, referring to the years in which the discharge presents values close to normal (Figure 4).

In both periods, for high discharge events, the increase in precipitation over the region relative to normal years is observed a few months in advance of the quarter of maximum discharge in NDJ (Figure 4). However, for events post-Salvajina (1987–2019), the December and January mean rainfall values exceed the monthly mean rainfall values of the pre-Salvajina by 23% and 26%, respectively. On the other hand, a slight decrease in the monthly mean rainfall for both periods occurs after August for low discharge events, with greater differences in December and January between pre-and-post-Salvajina. For these months, the decrease in total rainfall between the pre-and-post-Salvajina is approximately 10–17%.

Considering that on interannual scales, the main phenomenon associated with precipitation variations in the region is the ENSO [4,12,20], we find that pre-Salvajina, two high discharge events occurred during a strong La Niña, two during a moderate La Niña, and two during a weak La Niña, one during a neutral year, and one during a weak El Niño (Table 1). In contrast, post-Salvajina, five high events (62% of the cases) occurred during a strong La Niña, one during a moderate La Niña, and two during a weak La Niña. Meanwhile, pre-Salvajina, two low discharge events occurred during strong El Niño, three during weak El Niño, and three during neutral events. Post-Salvajina, two low discharge events occurred during a very strong El Niño, one during a strong El Niño, two during a moderate El Niño, one during a weak El Niño, and two in neutral years.

Furthermore, the annual cycle of the ONI index during high (low) discharge events at La Balsa station indicates a decrease (increase) in the intensity of SST anomalies in the region of the tropical Pacific post-Salvajina (Figure 5). For high discharge events (Figure 5a), during pre-Salvajina, SST anomalies between −0.6 and −0.9 (La Niña) are observed from September to April. However, for post-Salvajina events, SST anomalies are more intense

from August with values above −0.8, reaching the highest peak of anomalies in NDJ (between −1.3 and −1.37) until decaying in May. For low discharge events (Figure 5b), during pre-Salvajina, positive SST anomalies in the tropical Pacific (El Niño) higher than 0.5 and lower than 0.7 are observed from October to January. Nevertheless, post-Salvajina, SST anomalies higher than 0.8 are observed from August to February and only decay in April.

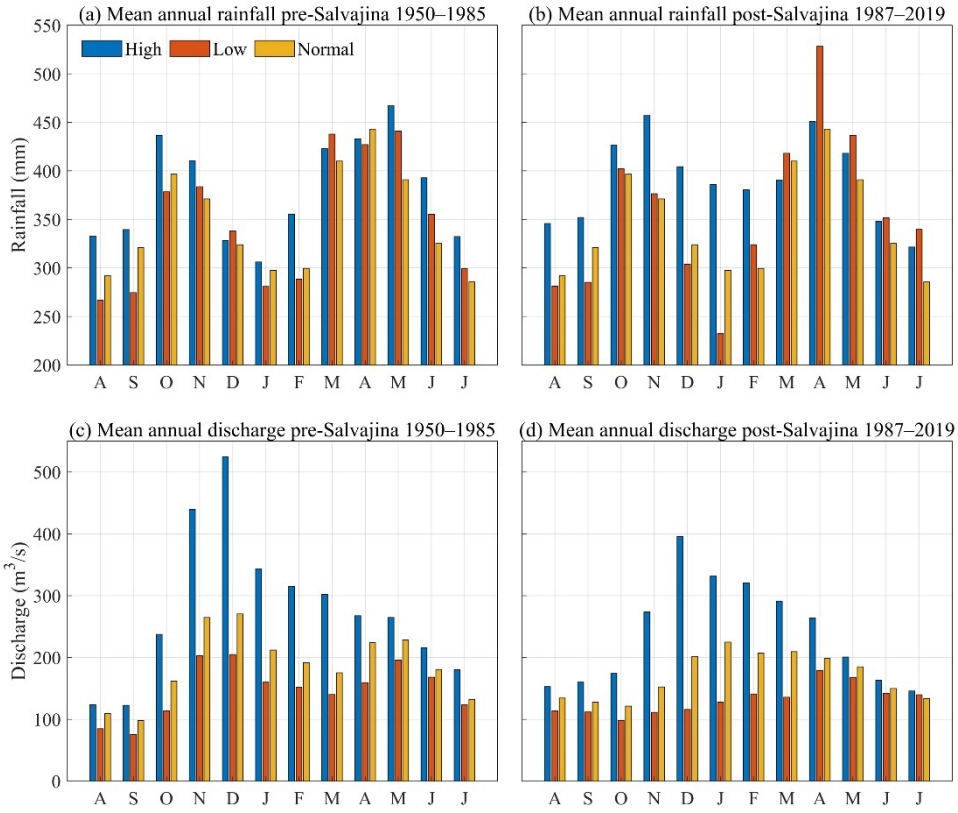


**Figure 4.** Annual mean precipitation cycle (**a**) before and (**b**) after the breakpoint, and annual mean discharge cycle (**c**) before and (**d**) after the breakpoint during high, low and normal discharge events. Blue bars for high discharge events, orange for low discharge events, and yellow for normal events. For precipitation the yellow bars correspond to the mean of all normal events between 1949–2019.

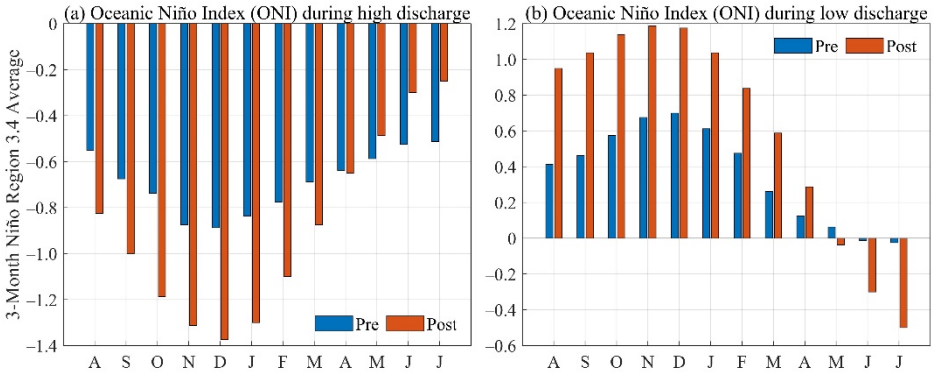


**Figure 5.** Annual cycle of the El Niño Ocean Index (ONI) during (**a**) high and (**b**) low discharge events, pre- and post-breakpoint. Blue bars for events pre-1986, and orange for events post-1986.

Results registered in Figures 4 and 5, and Table 1 show the ENSO influence on the hydrology in the study area, where the low (high) discharges are amplified during El Niño (La Niña) events, consistent with a reduction (increase) in precipitation (Figure 4). Behavior that Poveda et al. [29] reported in various gauging stations of rivers and rainfall throughout

Colombia during the 1970–2000 period, noting that the amplitude of the annual cycle of mean discharge and rainfall increases during La Niña, and decreases during El Niño. These results are also coherent with Ávila [23], who found in the Upper CRB positive and higher anomalies of the extreme precipitation indices during La Niña years than those during El Niño years. Furthermore, Ávila [23] reported nine flood events coinciding with the La Niña phenomenon during the 1970–2013 period, of which five (four) events occurred pre (post-) Salvajina Dam with flood areas ranging from 354–664 km$^2$ (83–440 km$^2$).

The findings of the direct relationship between discharge and precipitation where high (low) discharge peaks are related with maximum (minimum) precipitation peaks are due to the hydrological cycle of the watershed, considering that processes such as evapotranspiration, precipitation, run-off, and infiltration occur [14,87]. The results are consistent with the previous results found by Enciso et al. [4] and Canchala et al. [88]. Enciso et al. [4] showed that almost all areas with the highest precipitation throughout the Upper CRB coincided with the highest-specific-flow basins. Similar to the former research, Canchala et al. [88] also found a direct relationship between precipitation and the discharge of two basins of western Colombia (Atrato River and Patía River) where the greatest influence of the precipitation on streamflow was recorded synchronously, and the influence persisted up to 6 months later.

Therefore, a close association of high/low discharge events with increased/decreased precipitation during the NDJ may be associated with stronger La Niña/El Niño events observed post-Salvajina. To validate this, the following section uses the composite technique to evaluate the oceanic and atmospheric conditions of high and low discharge events pre- and post-Salvajina Dam.

### *4.2. Anomalous Sea Surface Temperature (SST) and Sea Level Pressure (SLP) Conditions Pre- and Post-Salvajina*

Figure 6 show the SST and SLP anomaly composites during pre-and-post-Salvajina (1986). High discharge events show significant negative SST anomalies in the tropical Pacific between 25° N–25° S, extending from the coasts of the Americas to 180° W (Figure 6a,b). However, the SST anomalies are more intense post-Salvajina, with a core of higher SST centered at the equator between 160° W–180° W, surrounded by positive SST anomalies in the western tropical and subtropical Pacific with the shape of a boomerang, setting up the typical La Niña SST pattern. Furthermore, negative SST anomalies are observed in the tropical North Atlantic (TNA) centered at 20° N and the Caribbean Sea pre-Salvajina, which are confined to the Caribbean Sea and the Gulf of Mexico post-Salvajina. Negative SST anomalies are also observed post-Salvajina in the tropical South Atlantic (TSA) centered at 20° S, and weak positive anomalies are observed along the northern coast of South America centered at the equator. These anomalous SST patterns contribute to the development of positive SLP anomalies in the central and eastern tropical Pacific between 40° N and 40° S and negative anomalies in the tropical Atlantic and western Pacific (Figure 6e,f). Nevertheless, post-Salvajina, these anomalies were more intense, and significant negative SLP anomalies were observed over most tropical South America. Thus, post-Salvajina, SLP anomalies defined a better configured zonal gradient between ocean basins due to the SST gradient between the western and central equatorial Pacific (negative SST anomalies) and the equatorial Atlantic (positive SST anomalies).

Moreover, the low discharge events exhibit a contrasting pattern of positive SST anomalies in the tropical Pacific (Figure 6c,d). Pre-Salvajina, this pattern was relatively weak and scattered in the tropical Pacific (Figure 6c), whereas, post-Salvajina, a well-configured SST positive anomaly pattern is observed over this oceanic region, extending from the coasts of South America and Central America, up to 180° W, with a core of large positive anomalies in the eastern Pacific, surrounded by negative anomalies in the western and subtropical Pacific, which is a typical El Niño pattern (Figure 6d). Positive SST anomalies are observed in the Atlantic basin for both cases, extending from the Caribbean towards TNA. However, post-Salvajina, these are more intense and widespread and result from the action of the El Niño in the TNA. Also, neutral to cold conditions

occur in the equatorial Atlantic for low discharge events post-Salvajina. Thus, a well-configured interbasin SLP gradient is evident only post-1986, with negative anomalies in the eastern and central tropical Pacific and positive anomalies in the eastern Pacific and equatorial Atlantic (Figure 6g,h). Interestingly, for high discharge events, the SST anomaly pattern post-Salvajina presents features of the La Niña event with higher anomalies in the western Pacific. In contrast, the low events present an El Niño SST pattern with the highest anomalies in the eastern Pacific. In this case, the SLP anomalies are more confined to the equator than those during high discharge events.

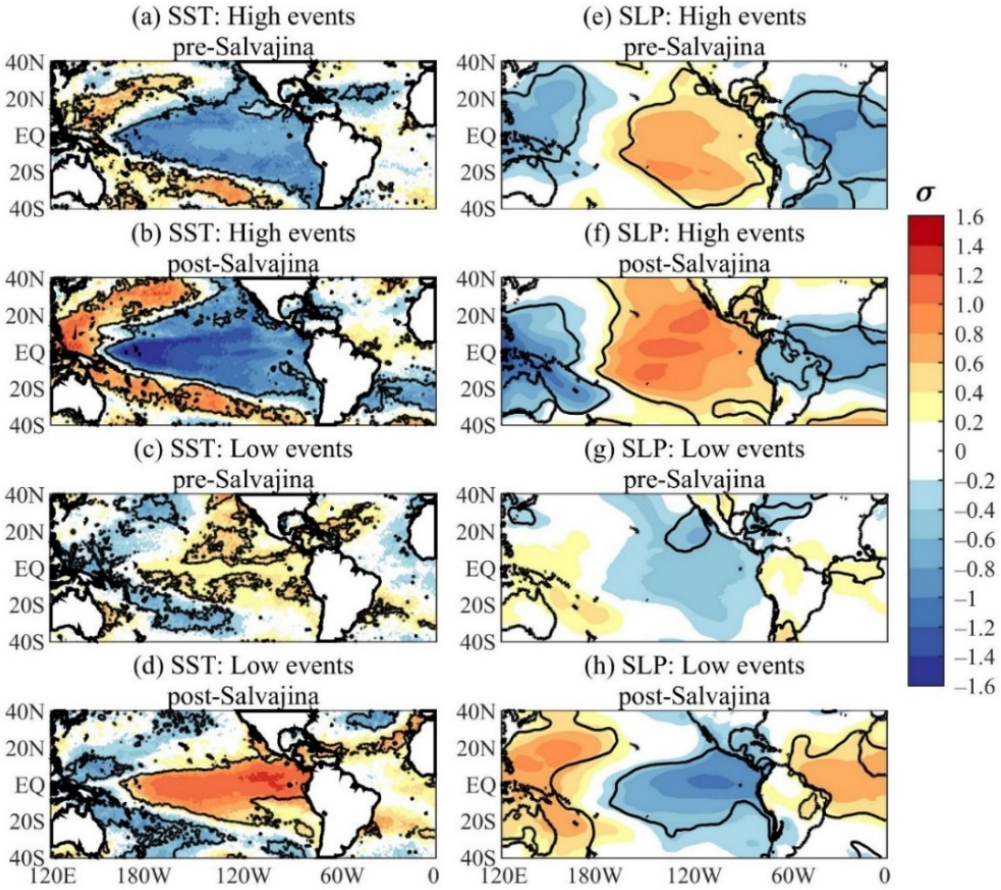


**Figure 6.** Standardized sea surface temperature (SST) anomalies associated with high discharge events (**a**) pre-Salvajina and (**b**) post-Salvajina, and low-discharge events (**c**) pre-Salvajina and (**d**) post-Salvajina. Standardized sea level pressure (SLP) anomalies associated with high discharge events (**e**) pre-Salvajina and (**f**) post-Salvajina, and low discharge events (**g**) pre-Salvajina and (**h**) post-Salvajina, at La Balsa station during November–January (NDJ). Shading interval: 0.2 SD. Continuous contours indicate significant values at a 95% confidence level.

The above results are coherent with Cai et al. [20] for the September–November, and December–February seasons. They found that the ENSO diversity directly influences the climatic impacts in western Colombia, such that central Pacific La Niña events have a stronger impact than eastern Pacific La Niña events (see their Figure 3) [20]. Similar results were found by Vicente-Serrano et al. [89] in the neighboring country of Ecuador, which reported that the SST anomalies in the central (eastern) Pacific regions are related to drought variability in the Andes (Western plains). Furthermore, it also observed that El Niño (La Niña) events enhance droughts in the Andes (Western plains) regions, evidencing a differentiated influence of the ENSO diversity on the droughts. According to Cai et al. [20], the climate and weather extremes probably increase in most regions of South America, given that the greenhouse warming induces the increase of occurrence of extreme La Niña

events [90]. Moreover, during low discharge events, a typical El Niño SST anomaly pattern is observed post-Salvajina, whereas it is not quite as evident in the pre-Salvajina period (Figure 6c,d). This result is due to the El Niño events observed in the post-Salvajina period being more intense than the events recorded during the pre-Salvajina period (Table 1 and Figure 5b), causing a decrease in precipitation and discharge in the CRB (Figure 4).

### *4.3. Anomalous Circulation, Precipitation, and Soil Moisture Conditions Pre- and Post-Salvajina*

Since the anomalous SST and SLP conditions suggest changes in flow discharge intensities pre- and post-1986 (Figure 6) since the construction of Salvajina Dam, it is expected that the atmospheric circulation from the Pacific and Atlantic to northwestern South America will also be altered. Figure 7 shows the wind vector at 925 hPa and the anomalous conditions of the zonal component for the events pre-and post-Salvajina. For the sake of understanding, the zonal component referred to as *u*, is the horizontal velocity component along a circle of latitude in a west-to-east direction. That is, when the *u* anomaly is positive, its trajectory is eastward, and vice-versa.

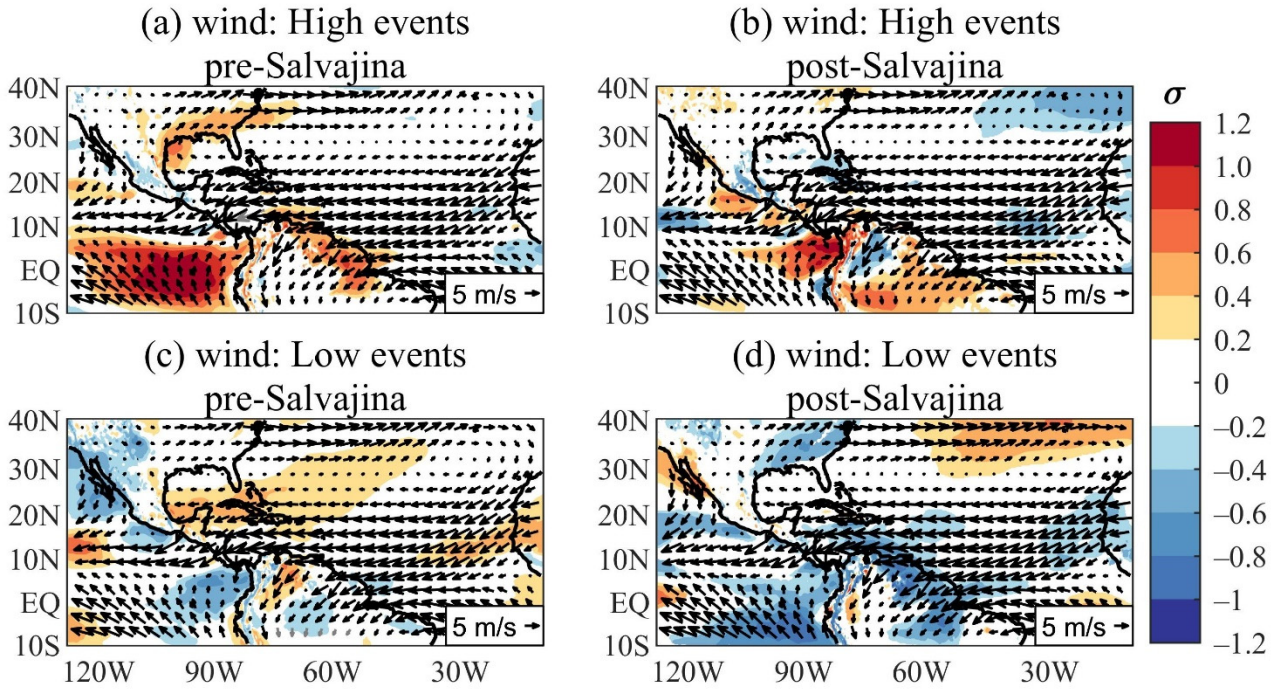


**Figure 7.** Composites of 925 hPa wind vector (m/s) and zonal wind standardized anomalies for November–January during: (**a**) high discharge events pre-Salvajina; (**b**) high discharge events post-Salvajina; (**c**) low discharge events pre-Salvajina; and (**d**) low discharge events post-Salvajina. Shading interval: 0.2 SD. Shaded areas indicate significant zonal wind anomalies at the 95% confidence level based on Student's t-test. Vectors in bold indicate significant magnitudes at 95% confidence level based on 'Student's *t*-test. The arrow at the bottom of these panels illustrates the base magnitude of the wind vector in m/s.

Figure 7a,b show a well-established circulation pattern associated with the Choco Jet (CJ) during periods of high discharge for the pre- and post-Salvajina years, with winds of 5–6 m/s centered around 80° W. In the TNA sector, northeasterly trade winds are visible, and in the Caribbean region, an east–west circulation pattern associated with the Caribbean low-level jet (CLLJ), with speeds varying between 8 and 12 m/s. Additionally, the anomaly pattern of the zonal wind component shows an intensification of westerlies in the eastern tropical Pacific region. However, there are differences in the positioning of these anomalies pre- and-post-Salvajina. Pre-Salvajina (Figure 7a), anomalous westerlies occur between 5° N and 10° S, and between the coast of Ecuador and Peru and 120° W; whereas, post-Salvajina (Figure 7b), the highest anomalous westerlies are centered over the Colombian Pacific, between the equator and 10° N, and between 90° W and 75° W, which

indicates a strengthening of winds in the area commonly known as the CJ core (between 2° N and 7° N and along 80° W) [7,11,18,22,91]. This result reflects a strengthening of the westerlies in the Colombian Pacific region post-Salvajina, which is associated with greater moisture transport from the eastern Pacific to the Colombian continental region. Furthermore, normal conditions are observed over the tropical Atlantic basin.

During low discharge events (Figure 7c,d), the atmospheric circulation at 925 hPa shows significant changes in the eastern Pacific region, where there is no establishment of the CJ-associated pattern due to anomalous 925 hPa easterlies, so a weakening of the CJ is expected. Moreover, the Caribbean and tropical Atlantic regions show contrasting results pre- and-post- Salvajina. Pre-Salvajina (Figure 7c), anomalous westerlies were observed in the Caribbean region, the Gulf of Mexico, and the western TNA between 20° N and 30° N, weakening the northeasterly trade winds and the CLLJ is expected in the Caribbean region; whereas, post-Salvajina (Figure 7d), anomalous 925 hPa easterlies are observed over most of the Caribbean and TNA, between the equator and 20° N, suggesting an intensification of the CLLJ, which tends to inhibit the formation of the CJ in the eastern Pacific.

Moreover, the precipitation anomaly patterns show a pronounced intensification over Colombia during the post-Salvajina high discharge events (Figure 8a,b), owing to the strengthening of the atmospheric circulation along the Colombian west coast, which strengthens the CJ. Pre-Salvajina, positive precipitation anomalies were limited to small areas of the Andes and the Colombian Caribbean, and over the Caribbean Sea along the Venezuelan coast (Figure 8a); post-Salvajina, larger positive precipitation anomalies were observed over central, western, and northern Colombia, with the largest anomalies occurring in the west, where the CRB is located (Figure 8b), as well as positive anomalies over most of the Caribbean Sea and the Pacific Ocean near the western Colombian coast. On the other hand, a pattern of negative anomalies is observed during low discharge events, with a greater extension over the Colombian Andes post-Salvajina (Figure 8c,d). Precipitation composites based on ERA5 (Figure 8) are also presented with GPCC (Figure A1 in Appendix A), with consistent results between the two datasets.

Our results are consistent with several studies that present evidence of the ENSO and CJ and CLLJ impact on rainfall and discharge variability over Colombia [22,29,91,92]. These studies show that, during La Niña, negative SST anomalies in the Pacific region strengthen the CJ and the moisture transport towards western and central Colombia, which coincide with high streamflow events pre- and post-Salvajina. On the other hand, during low discharge events associated with El Niño, mostly post-Salvajina, the reduction of the SST gradient between the eastern Pacific in the Niño 1 + 2 region and the Colombian Pacific weakens the CJ winds, decreasing the moisture advection towards the interior of Colombia, and the strengthening of the CLLJ due to positive SLP anomalies in TNA inhibit the formation of the CJ, which explains the more extended and intense negative precipitation anomalies post-Salvajina.

Moreover, Abelen et al. [93] and Wasko et al. [94] found that the soil moisture conditions may modulate changes in extreme hydrological conditions during extreme weather events. As soil moisture is closely related to precipitation and air moisture, it is expected from this variable complementary information about the events pre- and-post-Salvajina. For this reason, soil moisture composites were performed to examine how changes in this variable might have modulated the changes in high and low peak discharge post-Salvajina.

For high discharge events, an increase in positive soil moisture anomalies is observed over central, western, and northern Colombia post-Salvajina (Figure 9b), whereas pre-Salvajina, positive anomalies were only observed over the eastern and southwestern branches of the Colombian Andes (where the CRB originates; Figure 9a). Conversely, during low discharge events (Figure 9c,d), negative soil moisture anomalies are observed over the Colombian Andes post-Salvajina.

Figure 8 indicates that post-Salvajina the low (high) discharge events are linked to the negative (positive) precipitation anomalies which are larger in magnitude and extension than those recorded during the pre-Salvajina period in response to the more intense El

Niño events (more intense and frequent central La Niña events) after 1986. For high (low) discharge events, positive (negative) soil moisture anomalies in the post-Salvajina period imply a direct relationship between discharge and soil moisture (Figure 9), such as the lower (higher) soil moisture content increasing (decreasing) the soil's infiltration capacity, influencing in the reduction (augmentation) of flow in the basin. The results are coherent with Poveda et al. [14], who indicated that in the western, central, and northern Colombia, El Niño events are associated with a decrease in rainfall, a decrease in soil moisture, and a consequent decrease in the streamflow of the rivers, while that the opposite pattern was evidenced during La Niña events, which is characterized by the increase of the rainfall, increase of soil moisture, and subsequent increase of river flow. These results indicate that soil moisture plays a relevant role in the hydroclimatology of the basin, coherent with the statement of Poveda et al. [29] that soil moisture dynamics is a crucial component of climate variability over the tropical Andes from seasonal to interannual timescales.

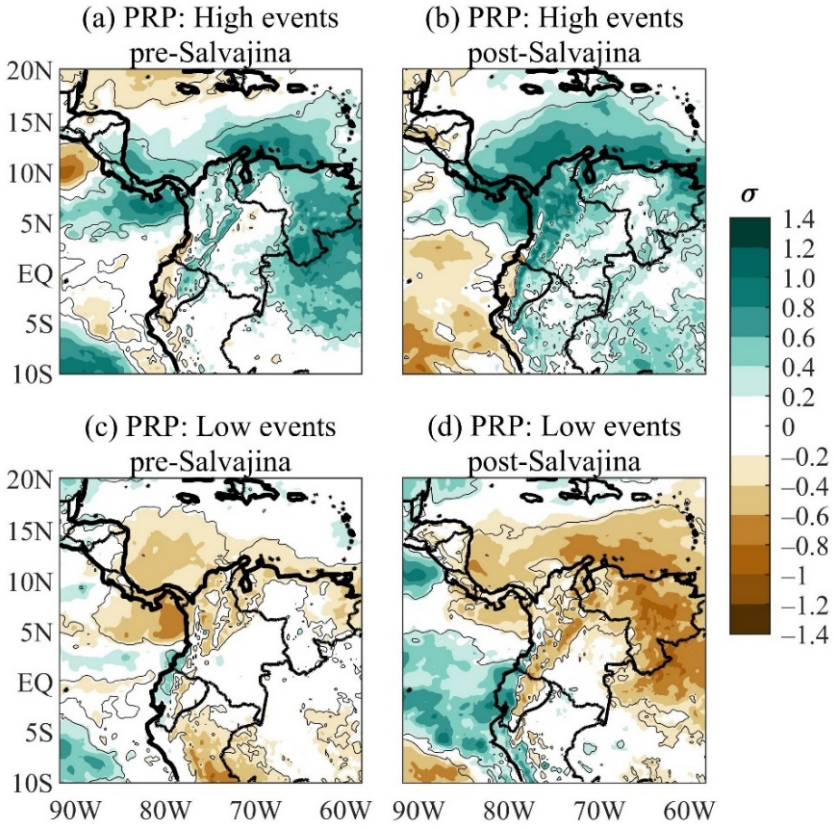


**Figure 8.** Standardized precipitation anomalies during (**a**) high discharge events pre-Salvajina; (**b**) high discharge events post-Salvajina; (**c**) low discharge events pre-Salvajina; and (**d**) low discharge events post-Salvajina. Shading interval: 0.2 SD. Continuous contours indicate significant values at the 95% confidence level.

Finally, after 1986, Colombia also has experienced negative socio-economic and environmental effects due to the extreme events of ENSO. During 1997–1998 and 2015–2016 El Niño events, two of the strongest on record, Colombia registered a collapse in coffee production (most important export crop), and an impact on 1 million hectares of crops in the Andean and Caribbean regions respectively, due to the decrease of rainfall in the country [49]. During La Niña events such as those registered in 2010–2012, extreme flooding occurred in the country, highlighting the disasters caused by the Cauca, Magdalena and Atrato Rivers [4,16,18].

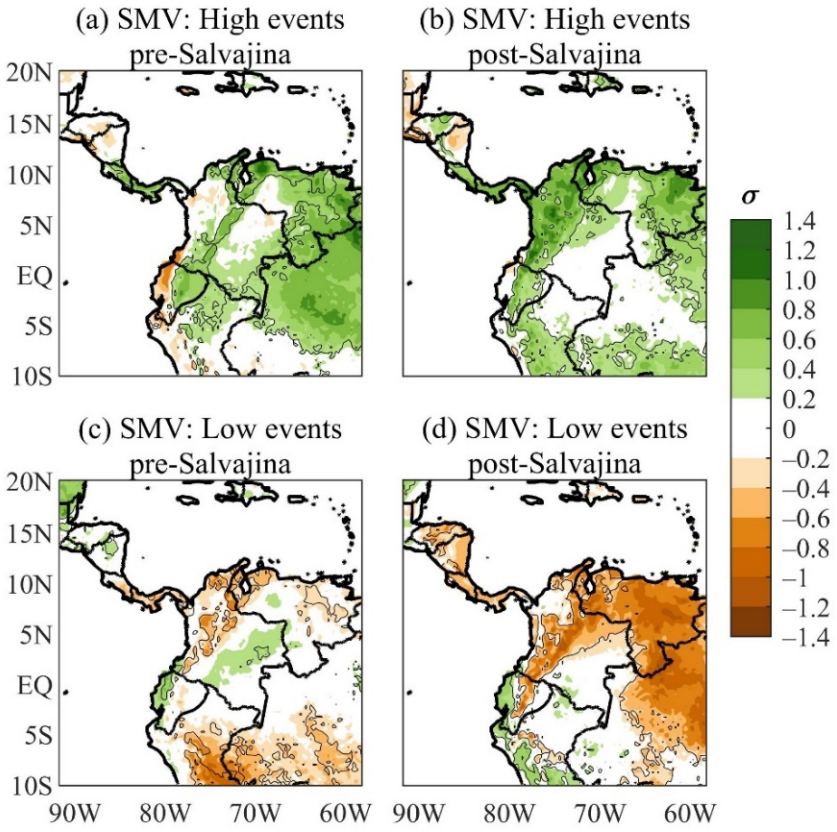


**Figure 9.** Standardized soil moisture volume (SMV) anomalies during (**a**) high discharge events pre-Salvajina; (**b**) high discharge events post-Salvajina; (**c**) low discharge events pre-Salvajina; and (**d**) low discharge events post-Salvajina. Shading interval: 0.2 SD. Continuous contours indicate significant values at 95% confidence level.

## 5. Conclusions

This research studied the hydroclimate variability of the Upper CRB at La Balsa Station, downstream of the La Salvajina hydroelectric facility, during 1950–2019 in Colombia. It adds to earlier studies by giving updated spatial and temporal coverage [4,23], using the newest datasets to assess meteorological patterns (e.g., ERA5 reanalysis) and observation (e.g., GPCC and in situ stations). The discharge time series for November–January (NDJ) during 1950–2019 shows a statistically significant downward break ($p < 0.05$) and change of distribution ($p < 0.001$) after 1986 associated with the operation of La Salvajina. Furthermore, our results highlight an association of high discharge events with increased precipitation during NDJ, which may be associated with more intense and frequent central La Niña events observed post-Salvajina and low discharge events linked to increased intensity of El Niño events post-1986 that reduced precipitation in the CRB. Indeed, more extreme climatic conditions were described post-Salvajina. This may raise the question that if the La Salvajina had not been completed in 1985, whether the floods and low water discharge would have been more pronounced due to the extreme conditions or not.

Please note this research did not include within its scope a hydraulic analysis of the Cauca River floods but aimed to evaluate possible changes in the spatiotemporal rainfall variability in the Upper CRB. As shown, an intensification of the rainfall evidences the necessity to use historical hydro-climatological data in the design of any dam and the use of future climate scenarios to improve flood control. Moreover, the mitigation of flood impacts in the basin requires a holistic approach. As reported by Restrepo [36], deforestation in the basin and the increase of socio-economic activities since 1985 in the valley could have also increased the floods' exposure in the last few years, reducing the flood control from La Salvajina.

**Author Contributions:** Conceptualization—W.L.C., M.T.K., A.A.-D., C.O.-M. and I.A.R. Methodology—W.L.C., A.A.-D., M.T.K., I.A.R. Software was managed by W.L.C., A.A.-D., I.P.d.S., I.A.R. and C.O.-M. Validation—W.L.C., A.A.-D., and M.T.K. Formal analysis—W.L.C., M.T.K., R.V.A., A.A.-D. and T.C. Investigation—W.L.C., M.T.K., R.V.A. and A.A.-D., Data curation—W.L.C., A.A.-D., I.A.R. and I.P.d.S. Original draft preparation—W.L.C., M.T.K., R.V.A., A.A.-D. and T.C. Reviewing and editing—W.L.C., M.T.K., R.V.A., A.A.-D. and I.A.R. Visualization—W.L.C. and A.A.-D. Supervision—W.L.C. All authors have read and agreed to the published version of the manuscript.

**Funding:** The first author was supported by the Universidad del Valle (Cali-Colombia). The Conselho Nacional de Desenvolvimento Científico e Tecnológico (CNPq) of Brazil partially supported the second, seventh and eighth authors under grants 302322/2017-5, 305611/2019-4, and 141982/2019-5, respectively. The seventh author was partially supported by Universidade do Estado do Amazonas (grant, ordinance 086/2021—GR/UEA). The sixth author has received funding from the CNPq under a Post-doctoral scholarship.

**Institutional Review Board Statement:** Not applicable.

**Informed Consent Statement:** Not applicable.

**Data Availability Statement:** Not applicable.

**Acknowledgments:** The authors are grateful to the Universidad del Valle (Cali-Colombia) and Universidade Federal de Itajubá. Thanks are also due to the The Conselho Nacional de Desenvolvimento Científico e Tecnológico (CNPq). All statistical tests were performed using statistical packages available in MATLAB R2021b (License: 40903835, Use-Option: Academic-Total Headcount, Master License: 31485653). The authors thank the three anonymous reviewers for their helpful comments.

**Conflicts of Interest:** The authors declare no conflict of interest.

## Appendix A

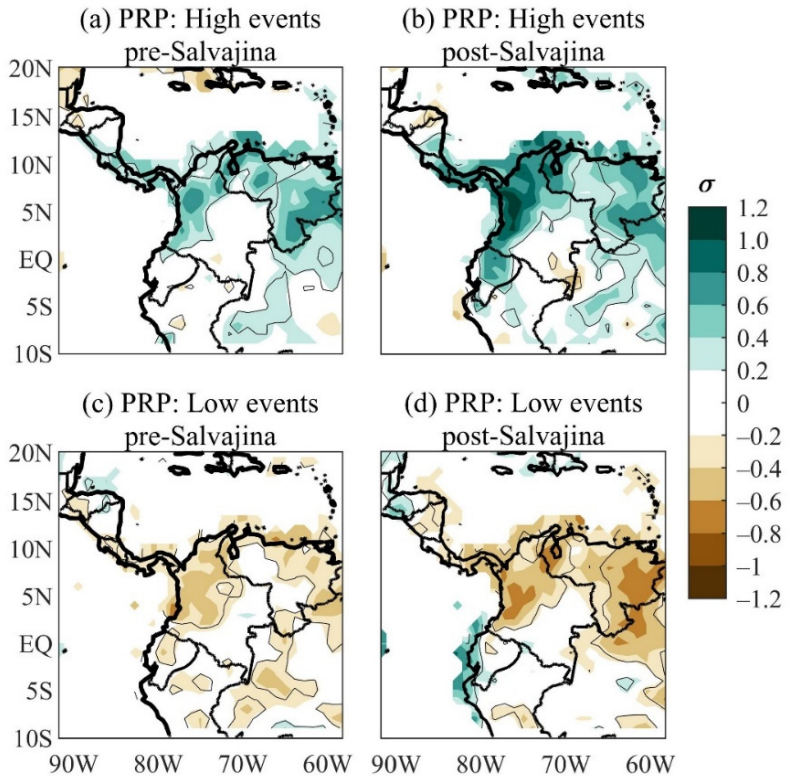


**Figure A1.** Standardized precipitation anomalies during: (**a**) high discharge events pre-Salvajina; (**b**) high discharge events post-Salvajina; (**c**) low discharge events pre-Salvajina; and (**d**) low discharge events post-Salvajina. Shading interval: 0.2 SD. Continuous contours indicate significant values at 95% confidence level. Based on Global Precipitation Climatology Center (GPCC) results.

## References


1. Gutiérrez, J.P.; van Halem, D.; Rietveld, L.C. Particulate matter characterization of Cauca River water in Colombia (preprint). *Hydrol. Earth Syst. Sci. Discuss.* **2016**, 1–20.
2. Valencia, J.M.; García, C.E.; Montero, D. Anomalías de vegetación asociadas con el fenómeno del ENOS en el valle geográfico del río Cauca, Colombia. *Rev. Teledetec.* **2017**, *2017*, 89–100. [CrossRef]
3. González-López, N.; Carvajal-Escobar, Y. Characterization of hydrological drought in the Cauca river high valley. *Tecnol. Cienc. Agua* **2020**, *11*, 235–264. [CrossRef]
4. Enciso, A.; Carvajal Escobar, Y.; Sandoval, M. Hydrological analysis of historical floods in the upper valley of Cauca river. *Ing. Compet.* **2016**, *18*, 46.
5. Sierra, J.P.; Arias, P.A.; Vieira, S.C. Precipitation over Northern South America and its seasonal variability as simulated by the CMIP5 models. *Adv. Meteorol.* **2015**, *2015*, 1–22. [CrossRef]
6. Pulwarty, R.S.; Barry, R.G.; Hurst, C.M.; Sellinger, K.; Mogollon, L.F. Precipitation in the Venezuelan Andes in the context of regional climate. *Meteorol. Atmos. Phys.* **1998**, *67*, 217–237. [CrossRef]
7. Poveda, G.; Jaramillo, L.; Vallejo, L.F. Seasonal precipitation patterns along pathways of South American low-level jets and aerial rivers. *Water Resour. Res.* **2014**, *50*, 98–118. [CrossRef]
8. Morales, J.; Arias, P.; Martínez, J. Role of Caribbean low-level jet and Choco jet in the transport of moisture patterns towards Central America. *Conf. Proc. Pap.* **2017**, *1*, 4861.
9. Bedoya-Soto, J.M.; Aristizábal, E.; Carmona, A.M.; Poveda, G. Seasonal Shift of the Diurnal Cycle of Rainfall Over Medellin's Valley, Central Andes of Colombia (1998–2005). *Front. Earth Sci.* **2019**, *7*, 92. [CrossRef]
10. Yepes, J.; Poveda, G.; Mejía, J.F.; Moreno, L.; Rueda, C. Choco-jex: A research experiment focused on the Chocó low-level jet over the far eastern Pacific and western Colombia. *Bull. Am. Meteorol. Soc.* **2019**, *100*, 779–796. [CrossRef]
11. Cerón, W.L.; Andreoli, R.V.; Kayano, M.T.; Souza, R.A.F.; Jones, C.; Carvalho, L.M.V. The Influence of the Atlantic Multidecadal Oscillation on the Choco Low-Level Jet and Precipitation in Colombia. *Atmosphere* **2020**, *11*, 174. [CrossRef]
12. Cerón, W.L.; Carvajal-Escobar, Y.; Andreoli, R.V.; Kayano, M.T.; González, N.L. Spatio-temporal analysis of the droughts in Cali, Colombia and their primary relationships with the El Niño-Southern Oscillation (ENSO) between 1971 and 2011. *Atmosfera* **2020**, *33*, 51–69. [CrossRef]
13. Montealegre, J.E.; Pabón, J.D. La Variabilidad Climática Interanual Asociada Al Ciclo El Niño-La Niña–Oscilación Del Sur Y Su Efecto En El Patrón Pluviométrico De Colombia. *Meteorol. Colomb.* **2000**, *2*, 7–21.
14. Poveda, G.; Jaramillo, A.; Gil, M.M.; Quiceno, N.; Mantilla, R.I. Seasonally in ENSO-related precipitation, river discharges, soil moisture, and vegetation index in Colombia. *Water Resour. Res.* **2001**, *37*, 2169–2178. [CrossRef]
15. Hoyos, I.; Baquero-Bernal, A.; Jacob, D.; Rodríguez, B. Variability of extreme events in the Colombian Pacific and Caribbean catchment basins. *Clim. Dyn.* **2013**, *40*, 1985–2003. [CrossRef]
16. Hoyos, N.; Escobar, J.; Restrepo, J.; Arango, A.; JC, O. Impact of the 2010-2011 La Niña phenomenon in Colombia, South America: The human toll of an extreme weather event. *Appl. Geogr.* **2013**, *39*, 16–25. [CrossRef]
17. Tedeschi, R.G.; Cavalcanti, I.F.A.; Grimm, A.M. Influences of two types of ENSO on South American precipitation. *Int. J. Climatol.* **2013**, *33*, 1382–1400. [CrossRef]
18. Arias, P.A.; Martínez, J.A.; Vieira, S.C. Moisture sources to the 2010–2012 anomalous wet season in northern South America. *Clim. Dyn.* **2015**, *45*, 2861–2884. [CrossRef]
19. Córdoba-Machado, S.; Palomino-Lemus, R.; Gámiz-Fortis, S.R.; Castro-Díez, Y.; Esteban-Parra, M.J. Influence of tropical Pacific SST on seasonal precipitation in Colombia: Prediction using El Niño and El Niño Modoki. *Clim. Dyn.* **2015**, *44*, 1293–1310. [CrossRef]
20. Cai, W.; McPhaden, M.J.; Grimm, A.M.; Rodrigues, R.R.; Taschetto, A.S.; Garreaud, R.D.; Dewitte, B.; Poveda, G.; Ham, Y.-G.; Santoso, A.; et al. Climate impacts of the El Niño–Southern Oscillation on South America. *Nat. Rev. Earth Environ.* **2020**, *1*, 215–231. [CrossRef]
21. Cerón, W.L.; Kayano, M.T.; Andreoli, R.V.; Canchala, T.; Carvajal-Escobar, Y.; Alfonso-Morales, W. Rainfall variability in Southwestern Colombia: Changes in ENSO—Related features. *Pure Appl. Geophys.* **2021**, *178*, 1–17. [CrossRef]
22. Cerón, W.L.; Andreoli, R.V.; Kayano, M.T.; Avila-Diaz, A. Role of the eastern Pacific-Caribbean Sea SST gradient in the Choco low-level jet variations from 1900–2015. *Clim. Res.* **2021**, *83*, 61–74. [CrossRef]
23. Ávila, Á.; Guerrero, F.C.; Escobar, Y.C.; Justino, F. Recent precipitation trends and floods in the Colombian Andes. *Water* **2019**, *11*, 379. [CrossRef]
24. Ocampo, C.; Carvajal-Escobar, Y.; Peña, L.E. Storm Water Management Model Simulation and Evaluation of the Eastern urban drainage system of Cali in the face of climate variability scenarios. *Ing. Compet.* **2019**, *21*, 1–11.
25. Ojeda-Flechas, C.D.; Burbano-Rodríguez, J.A.; Carvajal-Escobar, Y.; Hernández-Torres, F.L. Characterization of comprehensive drought events associated with the ENSO warm phase through satellite images in the Valle del Cauca, Colombia. *Dyna* **2020**, *87*, 204–214. [CrossRef]
26. Ocampo-Marulanda, C.; Carvajal-Escobar, Y.; Perafán-Cabrera, A.; Restrepo-Jiménez, L.M. Desiccation of Wetlands and Their Influence on the Regional Climate. Case Study: Ciénaga de Aguablanca, Cali, Colombia. *Trop. Conserv. Sci.* **2021**, *14*, 1–15. [CrossRef]

27. Bocanegra, R.A.; Stamm, J. Evaluation of alternatives to optimize the flood management in the department of Valle del Cauca. *J. Appl. Water Eng. Res.* **2021**, *9*, 1–19. [CrossRef]
28. Poveda, G. La hidroclimatología de Colombia: Una síntesis desde la escala inter-decadal hasta la escala diurna. *Rev. Acad. Colomb. Cienc.* **2004**, *28*, 201–222.
29. Poveda, G.; Álvarez, D.M.; Rueda, Ó.A. Hydro-climatic variability over the Andes of Colombia associated with ENSO: A review of climatic processes and their impact on one of the Earth's most important biodiversity hotspots. *Clim. Dyn.* **2011**, *36*, 2233–2249. [CrossRef]
30. Gutiérrez, F.; Dracup, J.A. An analysis of the feasibility of long-range streamflow forecasting for Colombia using El Niño–Southern Oscillation indicators. *J. Hydrol.* **2001**, *246*, 181–196. [CrossRef]
31. Vélez-Torres, I.; Vélez-Galeano, H. Acaparamiento del Agua y Despojo de la Tierra en el alto Cauca: Estudio Crítico Sobre (in)justicia Hídrica y Derecho al Agua en Colombia. *Nuestro Derecho al Agua Proy. del Planeta Azul*. Ottawa, ON, USA. 2012. Available online: https://biblioteca.cejamericas.org/bitstream/handle/2015/405/Nuestra_derecho_al_agua.pdf?sequence=1&isAllowed=y (accessed on 17 November 2021).
32. Velásquez, A.; Jiménez, N. La Gestión de Riesgos en el Ordenamiento Territorial: Inundaciones en Cali, la C.V.C. y el Fenómeno ENSO. In Proceedings of the Seminario Internacional Ambiental CVC 50 Años, Cali, Colombia, 13–17 September 2004; p. 18. Available online: https://www.osso.org.co/docu/congresos/2004/A_Velasquez_Articulo_OSSO-UV.pdf (accessed on 17 November 2021).
33. Perafán-Cabrera, A. Transformaciones paisajisticas en la zona plana vallecaucana. *Hist. Espac.* **2005**, *1*, 111–139. [CrossRef]
34. Armenteras, D.; Rodríguez, N.; Retana, J.; Morales, M. Understanding deforestation in montane and lowland forests of the Colombian Andes. *Reg. Environ. Chang.* **2011**, *11*, 693–705. [CrossRef]
35. Sanchez-Cuervo, A.M.; Aide, T.M. Identifying hotspots of deforestation and reforestation in Colombia (2001–2010): Implications for protected areas. *Ecosphere* **2013**, *4*, 1–21. [CrossRef]
36. Restrepo, J.D.; Kettner, A.J.; Syvitski, J.P.M. Recent deforestation causes rapid increase in river sediment load in the Colombian Andes. *Anthropocene* **2015**, *10*, 13–28. [CrossRef]
37. Capotondi, A.; Wittenberg, A.T.; Newman, M.; Di Lorenzo, E.; Yu, J.Y.; Braconnot, P.; Cole, J.; Dewitte, B.; Giese, B.; Guilyardi, E.; et al. Understanding ENSO diversity. *Bull. Am. Meteorol. Soc.* **2015**, *96*, 921–938. [CrossRef]
38. Yeh, S.W.; Kirtman, B.P. ENSO amplitude changes due to climate change projections in different coupled models. *J. Clim.* **2007**, *20*, 203–217. [CrossRef]
39. Dommenget, D.; Yu, Y. The effects of remote SST forcings on ENSO dynamics, variability and diversity. *Clim. Dyn.* **2017**, *49*, 2605–2624. [CrossRef]
40. Abish, B.; Cherchi, A.; Ratna, S.B. ENSO and the recent warming of the Indian Ocean. *Int. J. Climatol.* **2018**, *38*, 203–214. [CrossRef]
41. Wang, B.; An, S.I. A mechanism for decadal changes of ENSO behavior: Roles of background wind changes. *Clim. Dyn.* **2002**, *18*, 475–486.
42. Meehl, G.A.; Hu, A.; Santer, B.D. The mid-1970s climate shift in the pacific and the relative roles of forced versus inherent decadal variability. *J. Clim.* **2009**, *22*, 780–792. [CrossRef]
43. Restrepo, J.D.; Kjerfve, B. Magdalena river: Interannual variability (1975–1995) and revised water discharge and sediment load estimates. *J. Hydrol.* **2000**, *235*, 137–149. [CrossRef]
44. Comisión Económica para América Latina y el Caribe (CEPAL). *Valoración de Daños y Pérdidas: Ola Invernal en Colombia 2010–2011*; Naciones Unidas: Bogotá, Colombia, 2013; ISBN 9789585754409. Available online: https://repositorio.cepal.org/handle/11362/37958 (accessed on 17 November 2021).
45. Poveda, G.; Álvarez, D.M. El colapso de la hipótesis de estacionariedad por cambio y variabilidad climática: Implicaciones para el diseño hidrológico en ingeniería. *Rev. Ing.* **2012**, *36*, 65–76. [CrossRef]
46. Sedano-Cruz, K.; Carvajal-Escobar, Y.; Ávila, Á. Análisis de aspectos que incrementan el riesgo de inundaciones en Colombia. *Rev. Luna Azul* **2013**, *37*, 219–238.
47. Jacox, M.G.; Hazen, E.L.; Zaba, K.D.; Rudnick, D.L.; Edwards, C.A.; Moore, A.M.; Bograd, S.J. Impacts of the 2015–2016 El Niño on the California Current System: Early assessment and comparison to past events. *Geophys. Res. Lett.* **2016**, *43*, 7072–7080. [CrossRef]
48. Martínez, R.; Zambrano, E.; Nieto, J.J.; Hernández, J.; Costa, F. Evolución, vulnerabilidad e impactos económicos y sociales de El Niño 2015-2016 en América Latina. *Investig. Geográficas* **2017**, *68*, 65–78. [CrossRef]
49. Unidad Nacional para la Gestión del Riesgo de Desastres (UNGRD). In *Fenomeno El Niño. Análisis Comparativo 1997–1998//2014–2016*; Milena Mor: Bogotá, Colombia, 2016; ISBN 978-958-56017-0-3.
50. Corporación Autónoma Regional del Valle del Cauca—CVC. Centro Internacional de Agricultura Tropical—CIAT. In *Plan Integral de Cambio Climático para el Valle del Cauca PICC*; CVC and CIAT: Cali, Colombia, 2018. Available online: https://www.valledelcauca.gov.co/documentos/11533/plan-integral-de-cambio-climatico-del-valle-del-cauca-picc/ (accessed on 17 November 2021).
51. Departamento Administrativo Nacional de Estadística—DANE Censo Nacional de Población y Vivienda—CNPV. 2018. Available online: https://www.dane.gov.co/index.php/estadisticas-por-tema/demografia-y-poblacion/proyecciones-de-poblacion (accessed on 10 May 2021).
52. Puertas, O.O.; Carvajal-Escobar, Y.; Quintero, A.M. Estudio de tendencias de la precipitación mensual en la cuenca alta-media del río Cauca, Colombia. *Dyna* **2011**, *78*, 112–120.

53. Cerón, W.L.; Andreoli, R.V.; Kayano, M.T.; de Ferreria, S.R.; Canchala, N.T.; Carvajal-Escobar, Y. Comparison of spatial interpolation methods for annual and seasonal rainfall in two hotspots of biodiversity in South America. *An. Acad. Bras. Ciencias* **2021**, *93*, 1–22. [CrossRef] [PubMed]
54. Guzmán, D.; Ruíz, J.F.; Cadena, M. *Regionalización de Dolombia Según la Estacionalidad de la Precipitación Media Mensual, a Través Análisis de Componentes Principales (ACP)*; IDEAM: Bogotá, Colombia, 2014.
55. Corporación Autónoma Regional del Valle del Cauca—CVC. *Análisis Hidráulico de las Crecientes Históricas del Río Cauca*; Convenio de Asociación No.001 de 2013 ASOCARS—UNIVERSIDAD DEL VALLE: Cali, Colombia, 2013.
56. Hersbach, H.; Bell, B.; Berrisford, P.; Hirahara, S.; Horányi, A.; Muñoz-Sabater, J.; Nicolas, J.; Peubey, C.; Radu, R.; Schepers, D.; et al. The ERA5 global reanalysis. *Q. J. R. Meteorol. Soc.* **2020**, *146*, 1999–2049. [CrossRef]
57. Hoffmann, L.; Günther, G.; Li, D.; Stein, O.; Wu, X.; Griessbach, S.; Heng, Y.; Konopka, P.; Müller, R.; Vogel, B.; et al. From ERA-Interim to ERA5: The considerable impact of ECMWF's next-generation reanalysis on Lagrangian transport simulations. *Atmos. Chem. Phys.* **2019**, *19*, 3097–3214. [CrossRef]
58. Cerón, W.L.; Kayano, M.T.; Andreoli, R.V.; Avila-Diaz, A.; Ayes, I.; Freitas, E.D.; Martins, J.A.; Souza, R.A.F. Recent intensification of extreme precipitation events in the La Plata Basin in Southern South America (1981–2018). *Atmos. Res.* **2021**, *249*, 105299. [CrossRef]
59. Avila-Diaz, A.; Bromwich, D.H.; Wilson, A.B.; Justino, F.; Wang, S.-H. Climate Extremes across the North American Arctic in Modern Reanalyses. *J. Clim.* **2021**, *34*, 2385–2410. [CrossRef]
60. Yuan, P.; Hunegnaw, A.; Alshawaf, F.; Awange, J.; Klos, A.; Norman, F. Remote Sensing of Environment Feasibility of ERA5 integrated water vapor trends for climate change analysis in continental Europe: An evaluation with GPS (1994–2019) by considering statistical significance. *Remote. Sens. Environ.* **2021**, *260*, 112416. [CrossRef]
61. Aguirre, C.; Flores-Aqueveque, V.; Vilches, P.; Vásquez, A.; Rutllant, J.A.; Garreaud, R. Recent Changes in the Low-Level Jet along the Subtropical West Coast of South America. *Atmosphere* **2021**, *12*, 465. [CrossRef]
62. Gil Ruiz, S.A.; Barriga, J.E.C.; Martínez, J.A. Wind power assessment in the Caribbean region of Colombia, using ten-minute wind observations and ERA5 data. *Renew. Energy* **2021**, *172*, 158–176. [CrossRef]
63. Baker, J.C.A.; Castilho de Souza, D.; Kubota, P.Y.; Buermann, W.; Coelho, C.A.S.; Andrews, M.B.; Gloor, M.; Garcia-Carreras, L.; Figueroa, S.N.; Spracklen, D.V. An Assessment of Land–Atmosphere Interactions over South America Using Satellites, Reanalysis, and Two Global Climate Models. *J. Hydrometeorol.* **2021**, *22*, 905–922. [CrossRef]
64. Schneider, U.; Finger, P.; Meyer-Christoffer, A.; Rustemeier, E.; Ziese, M.; Becker, A. Evaluating the hydrological cycle over land using the newly-corrected precipitation climatology from the Global Precipitation Climatology Centre (GPCC). *Atmosphere* **2017**, *8*, 52. [CrossRef]
65. NOAA/ESRL/GPCC—National Oceanic and Atmospheric Administra-tion/Earth System Research Laboratory/Global Precipitation Climatology Centre Monthly Gridded Precipitation Data. Available online: https://psl.noaa.gov/data/gridded/ (accessed on 1 June 2021).
66. Pohlert, T. Non-Parametric Trend Tests and Change-Point Detection. Available online: https://mran.microsoft.com/snapshot/2016-06-30/web/packages/trend/vignettes/trend.pdf (accessed on 9 November 2021).
67. Mann, H.B.; Whitney, D.R. On a Test of Whether one of Two Random Variables is Stochastically Larger than the other. *Ann. Math. Stat.* **1947**, *18*, 50–60. [CrossRef]
68. Mann, H.B. Nonparametric Tests against Trend. *Econometrica* **1945**, *13*, 245–259. [CrossRef]
69. Kendall, M.G. *Rank Correlation Methods*; Griffin: London, UK, 1975; ISBN 0852641990.
70. Theil, H. A rank-invariant method of linear and polynomial regression analysis, 3; confidence regions for the parameters of polynomial regression equations. *Indag. Math.* **1950**, *1*, 467–482.
71. Theil, H. A Rank-Invariant Method of Linear and Polynomial Regression Analysis. In *Advanced Studies in Theoretical and Applied Econometrics*; Raj, B., Koerts, J., Eds.; Henri Theil's Contributions to Economics and Econometrics; Springer: Dordrecht, The Netherlands, 1992; Volume 23.
72. Sen, P.K. Estimates of the Regression Coefficient Based on Kendall's Tau. *J. Am. Stat. Assoc.* **1968**, *63*, 1379–1389. [CrossRef]
73. Avila-Diaz, A.; Justino, F.; Lindemann, D.S.; Rodrigues, J.M.; Ferreira, G.R. Climatological aspects and changes in temperature and precipitation extremes in viçosa-Minas Gerais. *An. Acad. Bras. Cienc.* **2020**, *92*, 1–19. [CrossRef] [PubMed]
74. Keggenhoff, I.; Elizbarashvili, M.; Amiri-Farahani, A.; King, L. Trends in daily temperature and precipitation extremes over Georgia, 1971-2010. *Weather Clim. Extrem.* **2014**, *4*, 75–85. [CrossRef]
75. Ahmad, I.; Tang, D.; Wang, T.; Wang, M.; Wagan, B. Precipitation trends over time using Mann-Kendall and spearman's Rho tests in swat river basin, Pakistan. *Adv. Meteorol.* **2015**, *2015*, 1–15. [CrossRef]
76. Yue, S.; Pilon, P.; Phinney, B.; Cavadias, G. The influence of autocorrelation on the ability to detect trend in hydrological series. *Hydrol. Process.* **2002**, *16*, 1807–1829. [CrossRef]
77. Pankaj, D. Pettitt Change Point Test for Univariate Time Series Data. Available online: https://www.mathworks.com/matlabcentral/fileexchange/60973-pettitt-change-point-test-for-univariate-time-series-data (accessed on 9 November 2021).
78. Fatichi, S. Mann-Kendall Test. Available online: https://www.mathworks.com/matlabcentral/fileexchange/25531-mann-kendall-test (accessed on 9 November 2021).
79. Tilgenkamp, A. Theil–Sen Estimator. Available online: https://www.mathworks.com/matlabcentral/fileexchange/34308-theil-sen-estimator (accessed on 9 November 2021).

80. Cardillo, G. MWWTEST: Mann-Whitney-Wilcoxon Non Parametric Test for Two Unpaired Samples. Available online: http://www.mathworks.com/matlabcentral/fileexchange/25830 (accessed on 9 November 2021).
81. Boschat, G.; Simmonds, I.; Purich, A.; Cowan, T.; Pezza, A.B. On the use of composite analyses to form physical hypotheses: An example from heat wave—SST associations. *Sci. Rep.* **2016**, *6*, 1–10.
82. Ananias, D.d.S.; de Souza, E.B.; Souza, P.F.S.; de Souza, A.M.L.; Vitorino, M.I.; Teixeira, G.M.; Ferreira, D.B.d.S. Climatologia da estrutura vertical da atmosfera em novembro para Belém-PA. *Rev. Bras. Meteorol.* **2010**, *25*, 218–226. [CrossRef]
83. Ayes Rivera, I.; Molina-Carpio, J.; Espinoza, J.C.; Gutierrez-Cori, O.; Cerón, W.L.; Frappart, F.; Armijos Cardenas, E.; Espinoza-Villar, R.; Ayala, J.M.; Filizola, N. The Role of the Rainfall Variability in the Decline of the Surface Suspended Sediment in the Upper Madeira Basin (2003–2017). *Front. Water* **2021**, *3*, 1–14. [CrossRef]
84. de Souza, I.P.; Andreoli, R.V.; Kayano, M.T.; Vargas, F.F.; Cerón, W.L.; Martins, J.A.; Freitas, E.; de Souza, R.A.F. Seasonal precipitation variability modes over South America associated to El Niño-Southern Oscillation (ENSO) and non-ENSO components during the 1951–2016 period. *Int. J. Climatol.* **2021**, *41*, 4321–4338. [CrossRef]
85. Wilks, D.S. *Statistical Methods in the Atmospheric Sciences*, 3rd ed.; Wilks, D.S., Ed.; Academic Press: San Diego, CA, USA, 2011; ISBN 9780123850232.
86. Panofsky, H.G.; Brier, G.W. *Some Applications of Statistics to Meteorology*; Mineral Industries Extension Services; College of Mineral Industries, Pennsylvania State University: State College, PA, USA, 1958.
87. Poveda, G.; Mesa, O.J. Feedbacks between hydrological processes in tropical South America and large-scale ocean-atmospheric phenomena. *J. Clim.* **1997**, *10*, 2690–2702. [CrossRef]
88. Canchala, T.; Cerón, W.L.; Francés, F.; Carvajal-Escobar, Y.; Andreoli, R.V.; Kayano, M.T.; Alfonso-Morales, W.; Caicedo-Bravo, E.; de Souza, R.A.F. Streamflow variability in colombian pacific basins and their teleconnections with climate indices. *Water* **2020**, *12*, 526. [CrossRef]
89. Vicente-Serrano, S.M.; Aguilar, E.; Martínez, R.; Martín-Hernández, N.; Azorin-Molina, C.; Sanchez-Lorenzo, A.; El Kenawy, A.; Tomás-Burguera, M.; Moran-Tejeda, E.; López-Moreno, J.I.; et al. The complex influence of ENSO on droughts in Ecuador. *Clim. Dyn.* **2017**, *48*, 405–427. [CrossRef]
90. Cai, W.; Wang, G.; Santoso, A.; Mcphaden, M.J.; Wu, L.; Jin, F.F.; Timmermann, A.; Collins, M.; Vecchi, G.; Lengaigne, M.; et al. Increased frequency of extreme La Niña events under greenhouse warming. *Nat. Clim. Chang.* **2015**, *5*, 132–137. [CrossRef]
91. Poveda, G.; Mesa, O.J. On the Existence of Lloró (the Rainiest Locality on Earth): Enhanced Ocean-Land-Atmosphere Interaction by a Low-Level Jet. *Geophys. Res. Lett.* **2000**, *27*, 1675–1678. [CrossRef]
92. Sierra, J.P.; Arias, P.A.; Vieira, S.C.; Agudelo, J. How well do CMIP5 models simulate the low-level jet in western Colombia? *Clim. Dyn.* **2018**, *51*, 2247–2265. [CrossRef]
93. Abelen, S.; Seitz, F.; Abarca-del-Rio, R.; Güntner, A. Droughts and floods in the La Plata Basin in soil moisture data and GRACE. *Remote Sens.* **2015**, *7*, 7324–7349. [CrossRef]
94. Wasko, C.; Nathan, R. Influence of changes in rainfall and soil moisture on trends in flooding. *J. Hydrol.* **2019**, *575*, 432–441. [CrossRef]